Fluorescence suppression in Raman spectroscopy using a time-gated CMOS SPAD

Juha Kostamovaara,^{1,*} Jussi Tenhunen,² Martin Kögler,² Ilkka Nissinen,¹ Jan Nissinen,¹ and Pekka Keränen¹

¹University of Oulu, Department of Electrical Engineering, Electronics Laboratory, FIN-90014 Oulu, Finland ²VTT Electronics, 90570 Oulu, Finland *juha.kostamovaara@ee.oulu.fi

Abstract: A Raman spectrometer technique is described that aims at suppressing the fluorescence background typical of Raman spectra. The sample is excited with a high power (65W), short (300ps) laser pulse and the time position of each of the Raman scattered photons with respect to the excitation is measured with a CMOS SPAD detector and an accurate timeto-digital converter at each spectral point. It is shown by means of measurements performed on an olive oil sample that the fluorescence background can be greatly suppressed if the sample response is recorded only for photons coinciding with the laser pulse. A further correction in the residual fluorescence baseline can be achieved using the measured fluorescence tails at each of the spectral points.

©2013 Optical Society of America

OCIS codes: (120.0120) Instrumentation, measurement, and metrology; (120.6200) Spectrometers and spectroscopic instrumentation; (300.6450) Spectroscopy, Raman.

References and links

- E. B. Hanlon, R. Manoharan, T.-W. Koo, K. E. Shafer, J. T. Motz, M. Fitzmaurice, J. R. Kramer, I. Itzkan, R. R. Dasari, and M. S. Feld, "Prospects for in vivo Raman spectroscopy," Phys. Med. Biol. 45(2), R1-R59 (2000).
- N. L. Jestel, "Process Raman spectroscopy," in Process Analytical Technology Spectroscopic Tools and Implementation Strategies for the Chemical and Pharmaceutical Industries (Blackwell, 2005), Chap. 5.
- R. Hopkins, S. H. Pelfrey, and N. C. Shand, "Short-wave infrared excited spatially offset Raman spectroscopy (SORS) for through-barrier detection," Analyst 137(19), 4408-4410 (2012).
- O. Khalil, "Spectroscopic and clinical aspects of noninvasive glucose measurements," Clin. Chem. 45(2), 165-
- 5. P. Matousek, M. Towrie, C. Ma, W. M. Kwok, D. Phillips, W. T. Toner, and A. W. Parker, "Fluorescence suppression in resonance Raman spectroscopy using a high-performance picosecond Kerr gate," J. Raman Spectrosc. 32(12), 983-988 (2001).
- K. Golcuk, G. S. Mandair, A. F. Callender, N. Sahar, D. H. Kohn, and M. D. Morris, "Is photobleaching necessary for Raman imaging of bone tissue using a green laser?" Biochim. Biophys. Acta 1758(7), 868-873 (2006).
- 7. R. P. Van Duyne, D. L. Jeanmaire, and D. F. Shriver, "Mode-locked laser Raman spectroscopy-a new technique
- for the rejection of interfering background luminescence signals," Anal. Chem. **46**(2), 213–222 (1974). D. V. Martyshkin, R. C. Ahuja, A. Kudriavtsev, and S. B. Mirov, "Effective suppression of fluorescence light in Raman measurements using ultrafast time gated charge coupled device camera," Rev. Sci. Instrum. 75(3), 630-635 (2004).
- E. V. Efremov, J. B. Buijs, C. Gooijer, and F. Ariese, "Fluorescence rejection in resonance Raman spectroscopy using a picosecond-gated intensified charge-coupled device camera," Appl. Spectrosc. 61(6), 571–578 (2007).
- 10. D. E. Schwartz, E. Charbon, and K. L. Shepard, "A single-photon avalanche diode array for fluorescence lifetime imaging microscopy," IEEE J. Solid State Circuits **43**(11), 2546–2557 (2008).

 11. I. Nissinen, J. Nissinen, A.-K. Länsman, L. Hallman, A. Kilpelä, J. Kostamovaara, M. Kögler, M. Aikio, and J.
- Tenhunen, "A sub-ns time-gated CMOS single-photon avalanche diode detector for Raman spectroscopy," in Proceedings of the European Solid-State Device Research Conference (ESSDRERC) (Institute of Electrical and Electronics Engineers, 2011), pp. 375–378.
- 12. Y. Maruyama, J. Blacksberg, and E. Charbon, "A 1024×8 700ps time-gated SPAD line sensor for laser Raman spectroscopy and LIBS in space and rover-based planetary exploration," in Proceedings of IEEE Conference on Solid-State Circuits (ISSCC) (Institute of Electrical and Electronics Engineers, New York 2013), pp. 110-111.
- 13. Y. Maruyama, J. Blacksberg, and E. Charbon, "A 1024 x 8, 700-ps time-gated SPAD line sensor for planetary surface exploration with laser Raman spectroscopy and LIBS," IEEE J. Solid State Circuits 49(1), 1–11 (2014).
- 14. I. Nissinen, A.-K. Lansman, J. Nissinen, J. Holma, and J. Kostamovaara, "2×(4×)128 time-gated CMOS single photon avalanche diode line detector with 100 ps resolution for Raman spectroscopy," in *Proceedings of the*

- European Solid-State Circuits Conference (ESSCIRC) (Institute of Electrical and Electronics Engineers, 2013), pp. 291–294.
- A. Rochas, M. Gani, B. Furrer, P. A. Besse, R. S. Popovic, G. Ribordy, and N. Gisin, "Single photon detector fabricated in a complementary metal—oxide—semiconductor high-voltage technology," Rev. Sci. Instrum. 74(7), 3263–3270 (2003).
- L. Pancheri and D. Stoppa, "Low-noise CMOS single-photon avalanche diodes with 32 ns dead time," in Proceedings of the European Solid-State Device Research Conference (ESSDRERC) (Institute of Electrical and Electronics Engineers, 2007), pp. 362–365.
- D. Stoppa, D. Mosconi, L. Pancheri, and L. Gonzo, "Single-photon avalanche diode CMOS sensor for timeresolved fluorescence measurements," IEEE Sens. J. 9(9), 1084–1090 (2009).
- 18. P. Keränen, K. Määttä, and J. Kostamovaara, "A wide range time-to-digital converter with 1ps single-shot precision," IEEE Trans. Instrum. Meas. **60**(9), 3162–3172 (2011).
- D. Bronzi, F. Villa, S. Bellisai, B. Markovic, S. Tisa, A. Tosi, F. Zappa, S. Weyers, D. Durini, W. Brockherde, and U. Paschen, "Low-noise and large-area CMOS SPADs with timing response free from slow tails," in Proceedings of the European Solid-State Device Research Conference (ESSDRERC) (Institute of Electrical and Electronics Engineers, 2012), pp. 230–233.
- M. A. Itzler, M. Entwistle, M. Owens, K. Patel, X. Jiang, K. Slomkowski, S. Rangwala, P. F. Zalud, T. Senko, J. Tower, and J. Ferraro, "Design and performance of single photon APD focal plane arrays for 3-D LADAR imaging," Proc. SPIE 7780, 77801M (2010).

1. Introduction

Raman spectroscopy is based on measurement of the intensity distribution of inelastically scattered photons from a monochromatic light source as a function of wavelength. Usually a CW (continuous wave) laser operating in the visible, near-infrared or near-ultraviolet range is used as a light source for illuminating the sample [1,2]. The laser light interacts with molecular vibrations and rotations in the sample system with the result that the energy (wavelength) of the scattered photons is shifted up or down (anti-Stokes or Stokes scattering). For a certain vibrational or rotational mode of a specific molecule, the change in the energy of the Raman scattered photon (the "Raman shift") is independent of the excitation photon energy. The Raman shift is typically expressed in wavenumbers [1/cm], i.e. as the difference between the excitation laser and the Raman emission wavenumbers. The Raman spectrum, i.e. the spectral distribution of the intensity of the Raman scattered photons, is unique for each chemical component and thus provides selectivity for a specific chemical component. Since the spectral distribution of the Raman scattering is a concentration-weighted linear combination of the Raman spectra of the pure components, the chemical composition of the sample can be calculated from the measured spectrum using chemometric calibration models [1]. Furthermore, dangerous components or counterfeit products can be identified in the sample.

Since absorption phenomena are weak in the VIS and NIR (visible and near-infrared) spectral regions where Raman spectroscopy is typically applied, Raman spectroscopy provides for easy and practical sampling, as does NIR spectroscopy, but where NIR spectroscopy yields information only on functional groups containing hydrogen (CH, OH, NH,..), the Raman spectrum provides a full set of vibrational and rotational spectral information, as typically obtainable only by combining the MIR and FIR (mid-infrared, farinfrared) spectroscopic techniques. On the other hand, Raman avoids the sampling difficulties entailed in these latter techniques, which result from the high absorption coefficients of the materials and the optical elements themselves within the wavelength regions concerned. For fibre-optic sampling, the spectral transmission of the fibre materials is even more suitable for Raman than for NIR spectroscopy, while in the case of MIR and FIR spectroscopies the technology for fibre-optic sampling is very limited and expensive [2]. Being the result of a scattering process, unlike NIR, MIR and FIR spectra, the Raman spectrum as measured through container walls, blisters, plastic bags, etc. provides information only on the enclosed material and not on the container, provided that the excitation and pick-up beams do not overlap at the container but only in the material that the package contains. This allows the contents to be studied without destroying or opening the packages [3]. Furthermore, Raman spectroscopy gives better resolved spectral lines, and since it has a low sensitivity for water, it is also better applicable to the study of biological and biochemical samples, which typically have a high water content [4].

Unfortunately, the measured Raman spectrum is typically masked by a strong fluorescence background in most potential applications. This is due to the fact that the probability of Raman scattering (cross-section) is much lower than that of fluorescence [1,2,5]. A strong fluorescence background gives rise to two problems. Firstly, it becomes the dominant element in the photon shot noise and thus detracts from the SNR (signal-to-noise ratio), and secondly, even if the Raman bands are narrow and the fluorescence has quite a smooth, featureless spectrum, errors in the mathematical estimation and removal (background subtraction) of the fluorescence increase with increasing fluorescence levels and result in increasing errors in both material identification and concentration measurement applications.

As a result, in spite of the obvious advantages of Raman spectroscopy, the strong fluorescence background has so far restricted its use in most otherwise potential applications in the agricultural, food and oil industries, security control and crime investigations, for example. Due to this limitation, Raman spectroscopy is nowadays generally used for the analysis of samples that do not absorb the excitation laser, "white powders" and synthetic, and thus clean, substances, e.g. in the pharmaceuticals industry.

An established laboratory practice for coping with the fluorescence problem given the existing instrumentation is "photobleaching", in which the specimen to be analysed is illuminated with the excitation laser over an extended period of time, typically several minutes, in order to destroy the fluorescent chromophores [6]. The method is nevertheless slow, it works only with some materials, it may induce chemical or physical changes in the samples and it certainly cannot be applied to living organisms.

Fluorescence has been effectively suppressed up to now by using near-infrared laser excitation, e.g. NdYAG 1064 nm, instead of the traditional shorter laser excitation wavelengths (400 nm – 830 nm), but this requires the use of InGaAs or Ge detectors, which produce dark current and read noise levels that are several orders of magnitude higher than the Si CCD which is predominantly used with traditional, shorter wavelength excitation (400 nm – 830 nm). This results in an increased noise level and a need for high excitation laser power (>1000 mW vs. typically a few tens to a few hundred mW with CCD-based systems) and long integration times (30 min to several hours vs. from a few seconds to a few minutes with CCD-based systems) [1].

Fortunately, since Raman scattering has a lifetime of much less than a picosecond, whereas fluorescence lifetimes are typically in the range of few thousand picoseconds or even tens of nanoseconds, it is possible to suppress the fluorescence background to a great extent if short, intensive laser pulses are used to illuminate the sample rather than CW radiation and the sample response is recorded only during these short pulses, see Fig. 1 and [5,7–9], for example, and references therein. Thus, by "time-gating" the measurement to the period of the laser pulse, the total intensity of the fluorescence in the recorded spectrum can be substantially reduced. This results in an improved signal-to-noise ratio and/or shorter measurement time, since the photon noise of the recorded fluorescence emission, which is proportional to the square root of the fluorescence baseline intensity, is now markedly reduced. Furthermore, the accuracy of the baseline of the Raman spectrum is improved, which also leads to greater accuracy in both material identification and quantitative analysis applications.

Several Raman spectrometer measurement set-ups that employ the above time-gating principle have been presented. For example, a high-speed optical shutter based on a Kerr cell is used to realize the time-gate function in [5] and [9], while a photo multiplier and a time gate fulfil the same purpose in [7]. The measurement of a time-gated Raman spectrum with a combination of a mode-locked laser, spectrograph and ICCD (intensified CCD) to achieve a 200ps temporal resolution has also been demonstrated [8]. Although functional in principle and able to demonstrate the potential of the time-gating method, the above systems are either highly sophisticated, physically large and expensive, or capable of measuring only a single wavelength band of the spectrum at a time, so that they require long measurement times and are thus unsuitable for off-laboratory applications.

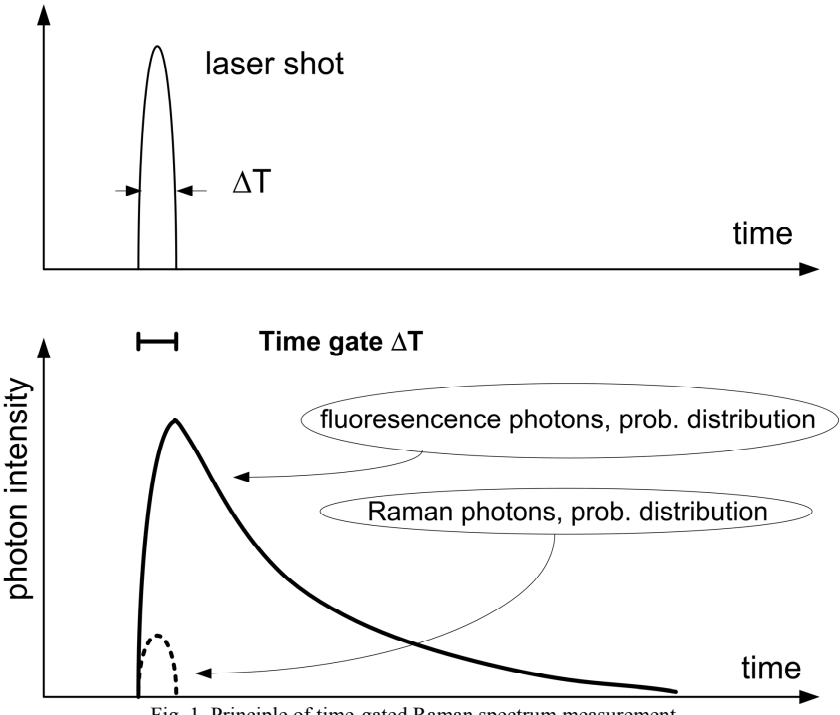


Fig. 1. Principle of time-gated Raman spectrum measurement.

We present here a measurement set-up which utilizes a time-gated CMOS single photon avalanche detector (SPAD) to determine the time position of the Raman scattered photons with respect to the laser shot. The results show that the width of the time gate can be less than 100ps, which results in a very efficient reduction in the fluorescence background, since this reduction is roughly proportional to the ratio of the time constant of the fluorescence emission to the width of the time gate. Moreover, since CMOS SPADs are realizable in 2D arrays, this method can be used for simultaneous measurement of the whole Raman spectrum by targeting each of the columns of the 2D detector array to a specific Raman wavelength band. Thus the method proposed here could pave the way to the development of a totally new family of Raman spectrometers intended for applications in which suppression of the fluorescence background is important.

Similar techniques based on measurement of the time position of photons with CMOS SPAD detectors have been used earlier in fluorescence studies, e.g. in [10]. The time-gating of a CMOS SPAD in Raman measurement was proposed and preliminarily demonstrated in [11], and then also in [12,13] with a CMOS SPAD 2D array having a minimum time-gate of 700ps. A 2D CMOS SPAD array with even shorter time gate was studied in [14]. Compared with [11] and [12,14], we present here a technique for measuring the complete 2D time interval - wavenumber spectrum of the sample, and especially for demonstrating the effectiveness of the sub-ns time-gating in achieving fluorescence suppression. Reference measurements obtained using other Raman spectrometer techniques are also shown.

2. Measurement configuration

2.1 Measurement principle

The measurement set-up and instrumentation used are shown in Fig. 2. A pulsed laser source is used to illuminate the sample. In order to maximize the effect of the time-gating and resulting fluorescence reduction, the laser pulse width should be at the limit of the system's time resolution. High average power is still needed to keep the measurement time reasonable, however, due to the low Raman scattering coefficient, and high spectral purity is also required for the sake of good spectral resolution. Our measurement system used a SHG (second harmonic) Nd:YAG micro-chip solid-state laser as the transmitter, with a wave length, pulse rate, pulse width and peak power of 532nm, 100kHz, 300ps (FWHM) and 65W, respectively.

In the proposed measurement set-up a single photon avalanche photon detector (SPAD) is used to detect the Raman scattered photons. This device, which can be realized in standard CMOS technologies [15–17], is basically a pn junction which is reverse-biased above its breakdown voltage, so that even a single photon entering the depleted region can trigger avalanche breakdown in the device. With a proper bias arrangement, the breakdown can directly produce a high-speed logic-level pulse for the measurement electronics without the need for a sensitive preamplifier. Thus this device is in fact a digital detector in nature (Geiger mode) and its sensitivity is limited by the shot noise of the signal and by the dark counts produced by thermal generation and any tunnelling effects. It should be noted, however, that in order to achieve a linear system response (in this case a Raman spectrum) using a Geiger mode detector, the probability of photon detection in a single laser pulse should be markedly less than one, which is typically the case in a Raman measurement due to the low Raman scattering coefficient.

The pulsed laser also triggers a delay generator, which enables the SPAD to operate during and after the laser pulse. Scattered photons are carried through an optical fibre to the spectrograph and to the SPAD-IC. Raman analysis is based on photons counted during a short time-gate window (ΔT in Fig. 1) overlapping with the laser pulse in order to suppress the fluorescence and effective dark count rate of the SPAD detector, the shot noise of which is one of the main noise sources affecting measurement. In this configuration a single CMOS SPAD detector was used so that in order to be able to measure the full Raman spectrum, the detector was moved at the output slit of the spectrometer (Imspector R6E by Specim Inc.) by means of a linear motor stage.

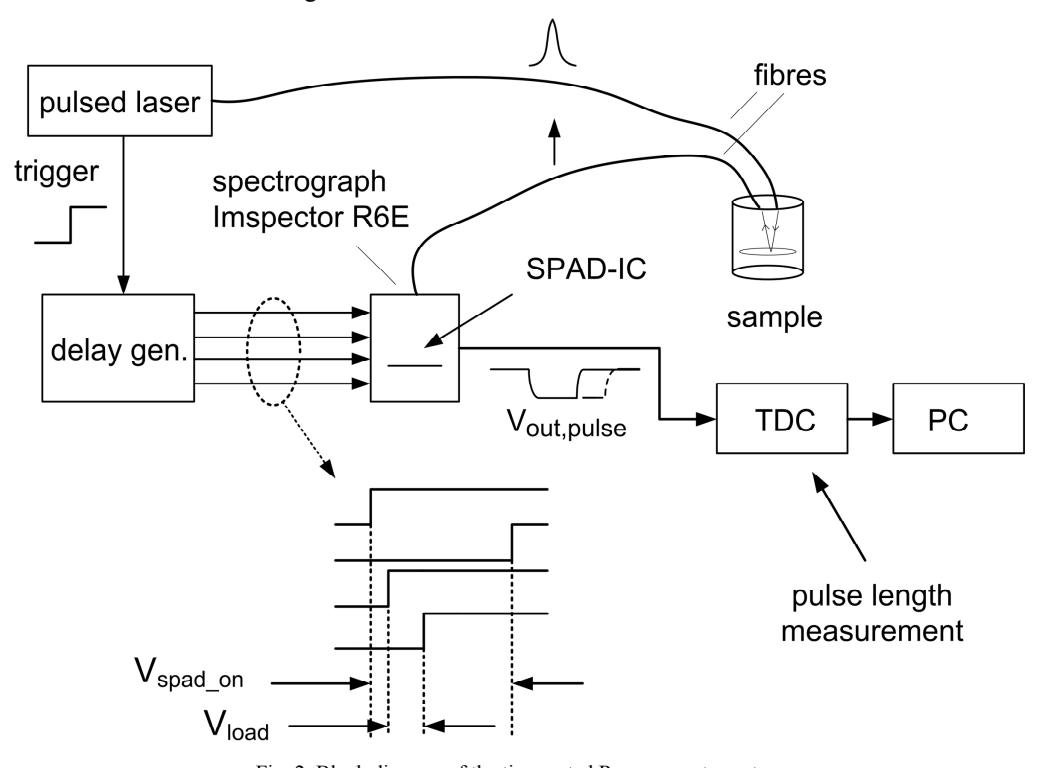


Fig. 2. Block diagram of the time-gated Raman spectrometer.

The SPAD chip was fabricated using $0.35 \mu m$ High Voltage CMOS technology and is similar to the structure in [17]. A cross-section of the SPAD chip is shown in Fig. 3. The

diode uses a deep-NWELL cathode and p + anode with a lightly doped p-well guard ring preventing surface breakdown. The SPAD is actively quenched and has a diameter of $20\mu m$ for its active area. The shallow depleted high-field region of the detector is quite narrow and thus the photon detection probability is typically only around 20-30%, peaking at about 500nm. On the other hand, due to this narrow depleted region, the time response is good, with a typical jitter of around 100ps (FWHM) [17]. Further details of the SPAD and its performance are given in [11].

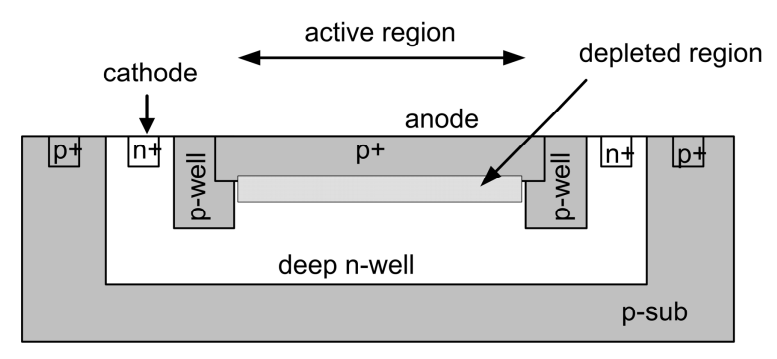


Fig. 3. Cross-section of the SPAD.

2.2 Time-gating

The schematic and timing diagrams of the SPAD are shown in Fig. 4 (and in Fig. 2). Its operation cycle is controlled via transistors M1 and M2, the operation of which is synchronized with the laser used to illuminate the sample. The bias voltage of the SPAD is kept below the breakdown limit with transistor M1, so that the diode is inoperative between the laser pulses. M1 is then switched off before the laser shot, with the result that the cathode of the SPAD will start to float. The cathode is then biased above the breakdown voltage $(V_B + V_{CC} > V_{BR})$ just before the laser pulse with transistor M2, which is switched ON with a short (<1ns) V_{load} pulse. Thus the diode is ready to detect photons after the trailing edge of the V_{load} .

The breakdown of the SPAD induced by the detected photon or active quenching of the SPAD (trailing edge of V_{spad_on}) resets its cathode voltage and restarts the operation cycle. As a result, the output of the inverter $V_{out,pulse}$ is a pulse with its leading edge produced by a signal synchronized with the laser shot and trailing edge by the detected photon (or the start of the active quenching cycle). Thus, the time position of the photon with respect to the laser pulse can be determined by measuring the duration of this pulse. All the system time offsets, including that produced by the finite length of T_{load} , can easily be adjusted by recording the laser-induced photons scattered from the sample at the laser wavelength during a separate calibration period. In this measurement configuration an accurate off-chip time-to-digital (TDC) converter circuit was used to measure the length of the $V_{out,pulse}$. This TDC circuit has a single shot precision of about 1 to 2ps (sigma value), representing the uncertainty of the pulse width measurement [18].

The pulses V_{load} and V_{spad_on} were generated with an on-chip pulse generator having four input pulses from an external adjustable delay generator triggered by the pulsed laser, as shown in Fig. 2. The time differences between these input signals were externally adjusted so that the desired pulse widths could be achieved at the inputs to the SPAD (V_{load} and V_{spad_on}). The width T_{load} of the V_{load} that pulls the SPAD anode into the "detection mode" was less than 500 ps.

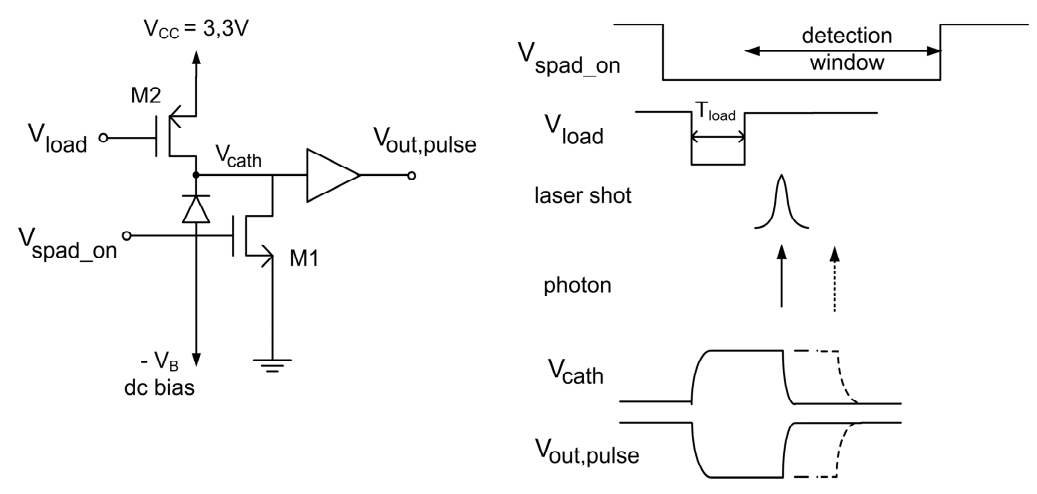


Fig. 4. Control circuit and timing diagram of the SPAD.

It should be noted that the measurement configuration presented here enables not only time-gating but also measurement of the time positions of all the laser-induced photons, as a function of the wavelength if the detector were realized as a 2D array, see Fig. 5. Thus all the signal processing necessary to analyse the results can be done using software. For example, if one is only interested in the Raman spectrum a time window corresponding to the Raman photons (overlapping with the laser pulse) can be employed, and its fluorescence background can even be corrected based on estimates of the measured number of photons detected as a function of time, (or vice versa) based on the fluorescence part (photons detected after the laser shot). Since the time positions of all the detected photons are recorded accurately, flexible post-processing of the results is obviously possible, and in principle it is also possible to enable the SPAD only through its supply voltage, but then gating periods of less than a few hundreds of picoseconds may become impractical due to difficulties in realizing short, subnanosecond logic-level pulses for a large capacitive load.

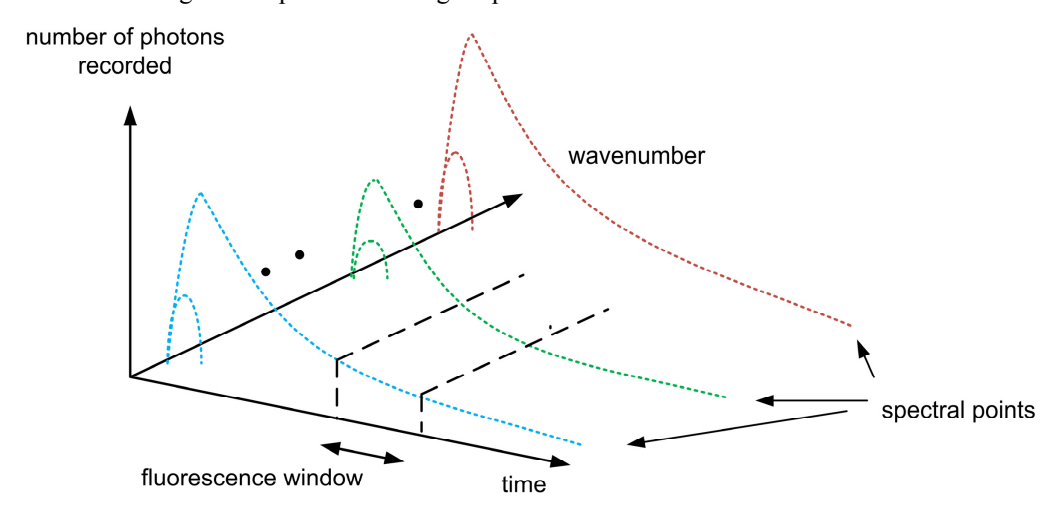


Fig. 5. Raman and fluorescence spectra as functions of wavelength and time.

3. Measurement results

The functionality of the time-gated Raman spectrometer was tested using olive oil, which is known to produce a strong fluorescence background. The excitation wavelength, pulsing frequency, pulse energy and recording time for this measurement were 532nm, 100kHz, 20nJ

and 240 seconds (per one spectral point), respectively. About 630 points were recorded in the spectrum within a wavelength region of 538 - 646nm. The time positions of the recorded photons at these spectral points were measured with a TDC (time-to-digital converter). The normalized number of recorded photons is shown in Fig. 6 as a function of the wavenumber and the time difference between the laser shot and the recorded photon.

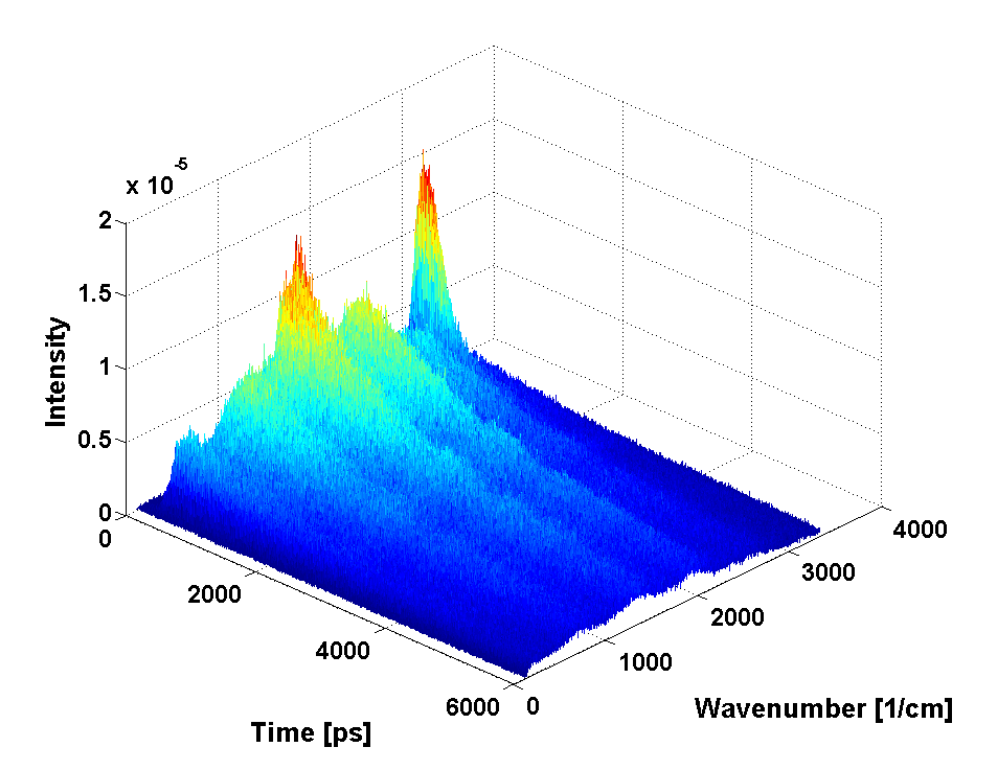


Fig. 6. Number of photons (normalized) recorded as a function of the wavenumber and the time interval relative to the laser shot.

Several Raman spectra were then calculated using time-gate windows of differing widths, as shown in Fig. 7, each spectral point being achieved by integrating the total number of photons recorded at that point as a function of time within the corresponding time window starting from a time position of 250ps (at the leading edge of the laser pulse) and normalizing this number to the total number of laser shots at that spectral point (which was $240 \text{sec} * 100 \text{kHz} = 2.4 * 10^7 \text{ shots on average}$).

As may be seen, with a gate window width of 6ns the Raman spectrum is strongly masked by the fluorescence and the whole measured spectrum is modulated as a function of wavelength by interference from the dielectric layers on the top of the detector (persisting even after removal of the on-chip passivation layer). However, by reducing the gate width to a sub-ns range, more and more Raman features could be visualized due to the reduction in fluorescence. The fluorescence background was already greatly suppressed with gate window widths of 100ps and 50ps, although the signal-to-noise ratio (SNR) was also reduced, especially with the 50ps gate window width, due to the lower number of photons recorded.

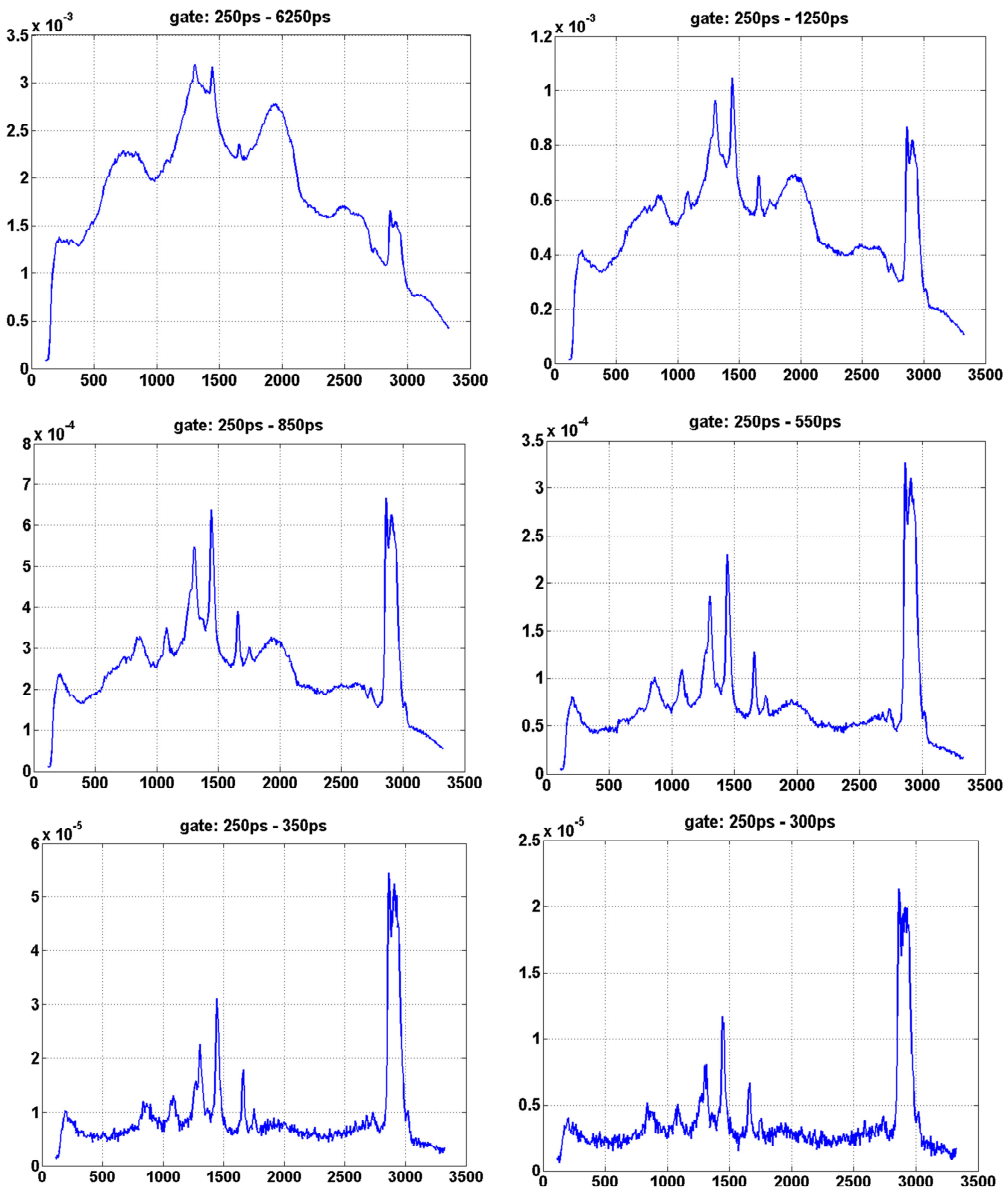


Fig. 7. Raman spectra measured with time gate widths of 6ns (from 250ps to 6250ps), 1ns (from 250ps to 1250ps), 600ps (from 250ps to 850ps), 300ps (from 250ps to 550ps), 100ps (from 250ps to 350ps) and 50ps (from 250ps to 300ps). x-axis: wavenumbers [1/cm] and y-axis: relative intensity.

In addition to the time gating, it is also possible to estimate the residual fluorescence (fluorescence photons arriving within the same time window as the Raman scattered photons) based on the measured fluorescence tail at each of the spectral points and further subtract this from the total number of photons within the time gate window. This method is demonstrated in Fig. 8, where curve 1 (blue) shows the uncompensated Raman spectrum measured with a time gate window of 600ps (as in Fig. 7), curve 2 (red) shows the calculated fluorescence background based on the measured fluorescence counts within a window of 600ps located 3ns after the laser shot, see Fig. 5, and curve 3 (green) shows the compensated Raman spectrum, which is the difference between these two results. The compensation curve (red) is just a scaled (constant scaling coefficient in all spectral points) version of the measured

fluorescence spectrum. It was thus assumed in the calculation that the time constant of the fluorescence does not change along the spectrum.

Interestingly, the interference seen in the measured spectra, most notably in curve 2, is actually also a demonstration of the capability of a single photon to interfere with itself. The differences between the interference minima and maxima (about 350 1/cm) correspond quite well to the approximate thickness of the dielectrics (9-10um) from the top metal down to the junction of the SPAD detector.

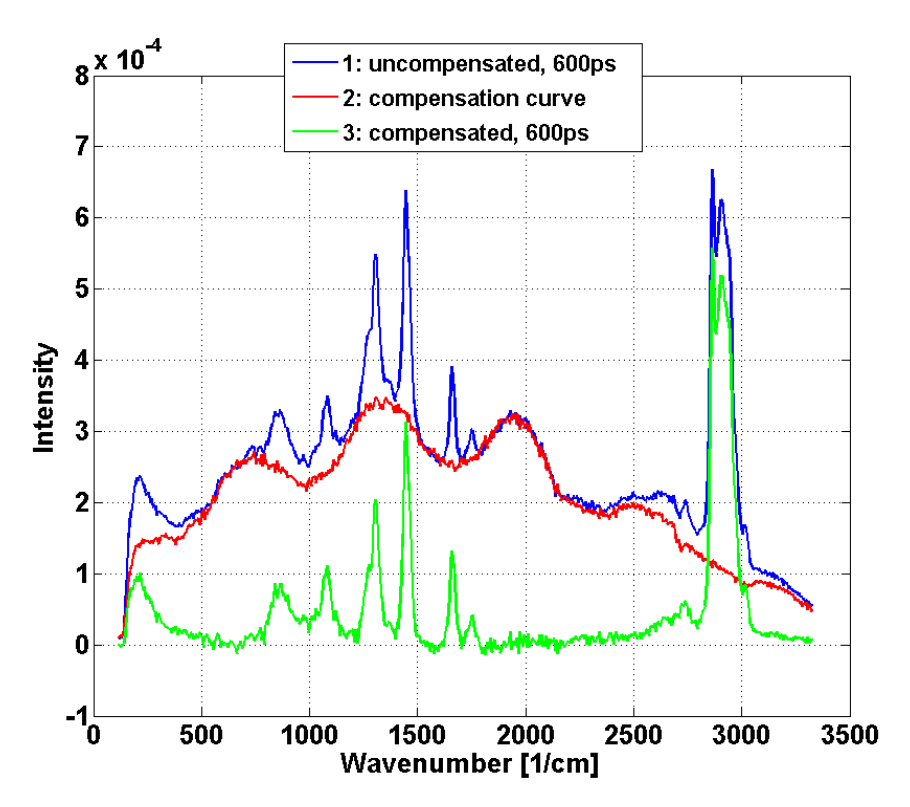


Fig. 8. Curve 1 (blue): uncompensated Raman spectrum measured with a time gate window of 600ps; curve 2 (red): calculated fluorescence background based on the measured fluorescence counts within a window of 600ps located 3ns after the laser shot; curve 3 (green): fluorescence-compensated Raman spectrum, i.e. the differences between curves 1 and 2.

A result representing a more complete estimate for the fluorescence background based on fitting of the convolution of the instrumental function and exponential fluorescence decay with a single time constant is shown in Fig. 9. In Fig. 9 panel a shows the distribution of Raman photons after fluorescence correction and panel b the Raman spectrum calculated from the result of panel a within a time window of 250ps – 900ps. The results of Figs. 8 and 9 are interesting since they point to a better signal-to-noise ratio than is achievable with pure gating using the shortest gate window widths, see Fig. 7.

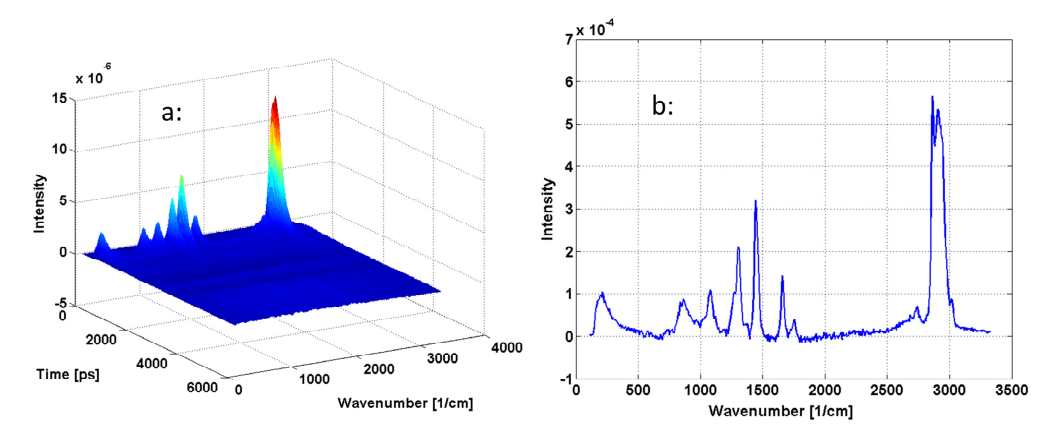


Fig. 9. a) Intensity of Raman photons after fluorescence correction as a function of the wavenumber and the time interval relative to the laser shot; b) Raman spectrum calculated from Fig. 9(a) within a time gate of 250ps - 900ps.

The result presented in Fig. 10 is an attempt to clarify the difference in full time behaviour between the recorded Raman and fluorescence photons. It shows the time positions of the recorded photons with respect to the laser pulse at three wavenumbers. Curve 1 (red) was measured at a wavenumber of 1444 1/cm, which coincides with the strongest Raman peak, whereas curves 2 (green) and 3 (blue) were recorded at wavenumbers of 1940 1/cm and 2183 1/cm, respectively, which are free from Raman. The fluorescence spectrum is similar in curves C1 and C2 and thus the contribution of the Raman photons is seen as their difference, as shown by the black curve 4. The fluorescence curves can be regarded as convolutions with the instrumental function (defined by the laser pulse width and the time response of the SPAD detector), while the time distribution of the Raman photons follows the shape of the instrumental function. Thus curve C4 also illustrates the instrumental function of the measurement, its width being approximately 350ps FWHM (full width, half maximum).

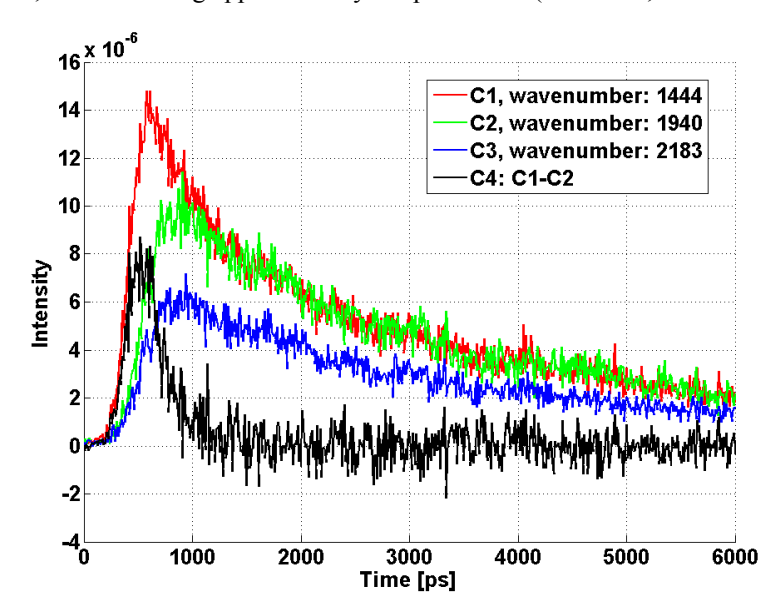


Fig. 10. Time distributions of the number of photons recorded at the position of the Raman peak (C1, red curve) and Raman free spectral points (C2 and C3, green and blue curves). The black curve C4 indicates the difference between the red and green curves.

Another measurement was performed to compare the results obtained by the time-gated SPAD-based techniques with those of the standard Raman spectroscopic techniques. First, a reference spectrum was recorded with a standard 2D CCD detector-based (Andor Newton DU-971N_BV) CW Raman system using an excitation wavelength, average laser power and total integration time of 785nm, 350mW and 1 second, respectively. Curve 1 (red) in Fig. 11 shows the number of photons recorded as a function of the Raman shift in wavenumbers compared with the laser line from the olive oil sample. As may be seen, the spectrum is dominated by fluorescence and the Raman scattered photons produce only a slight variation in the recorded intensity.

Curve 2 (green) shows the recorded time-gated Raman spectrum using the time-gated SPAD-based measurement system described above. In this measurement the excitation wavelength, average laser power and recording time were 532nm, 2mW and 240 seconds (per pixel), respectively. Each point of the spectrum was produced by counting the recorded photons only during a time window of 500ps positioned to overlap with the laser pulse. In addition, this number was corrected (reduced) by estimating the number of fluorescence photons during the window based on the distribution of fluorescence after the laser shot. As may be seen, the Raman peaks in the time-gated SPAD detector-based spectrum correspond quite well to the results of the CW Raman system. This finding was further confirmed by repeating the measurement with a commercial FTIR (Fourier transform infrared spectroscopy) Raman system (Bruker Optics, MultiRAM II), which is capable of largely avoiding the fluorescence background by using an NIR wavelength for sample excitation (1064nm). Unfortunately, this method is not suitable for off-laboratory use because of its long measurement time, complexity and cost. Again the FTIR result, curve 3 (blue), achieved using an excitation wavelength, average power and measurement time of 1064nm, 1200mW and 1200 seconds, confirms the results obtained with the time-gated CMOS SPAD-based Raman spectrometer.

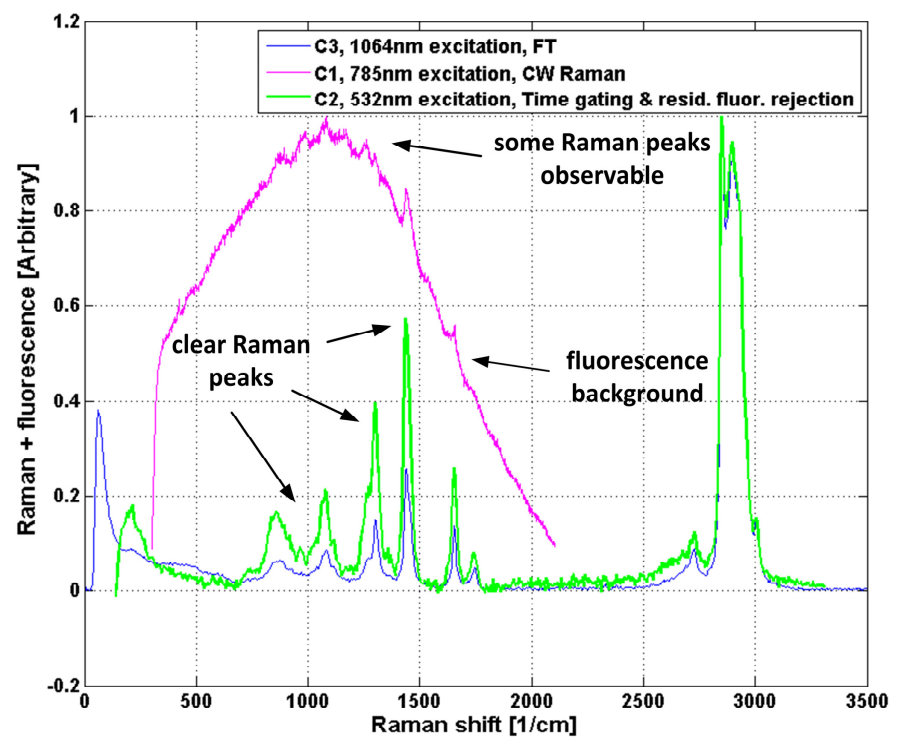


Fig. 11. Raman spectra recorded for an olive oil sample. Red curve C1 based on standard CW Raman measurement, green curve C2 based on time-gated CMOS SPAD measurement, and blue curve C3 based on FTIR measurement.

4. Discussion and conclusions

In a conventional Raman spectrometric measurement the signal-to-noise ratio (SNR) of the result is defined by the shot noise of the events recorded in a particular wavelength channel. The total number of these includes not only the scattered Raman photons but also the background radiation and especially photons introduced by fluorescence from the sample. It should be noted that while the average fluorescence and background levels can be estimated quite reliably and subtracted from the spectrum, their shot noise (randomness in the number of recorded photons) still remains after baseline correction, see Eq. (1):

$$SNR_{channel} = \frac{N_{Raman_photons}}{\sqrt{N_{Raman_photons} + N_{Background} + N_{fluor}}}$$
(1)

Thus, in order to maximize the SNR, it would be important to suppress all detections other than Raman scattered photons. We have shown in this work is that with a simple and cheap CMOS SPAD (single photon avalanche detector) it possible to realize a time-gating function in the sub-nanosecond range, which then results in strong fluorescence suppression that is typical of Raman spectrometer measurements.

By separating the spectra of Fig. 7 in the manner shown in Fig. 8 for one specific time gate length and then integrating the Raman and fluorescence contributions over the spectrum (wavenumber) it is possible to evaluate the total probability of different types of detections in this particular measurement arrangement. Such a calculation shows that the detection probabilities for fluorescence and Raman photons within the whole spectrum in this measurement arrangement are 53% and 2.7%, respectively, for a gate length of 6ns and 12% and 2.9% for a time gate of 600ps. Upon shortening the time gate to 300ps, the detection probabilities go down to 2.9% for the fluorescence and 1.6% for the Raman photons. Thus their proportion changes approximately by a factor of 10 due to the time gating with 300ps, which is in accordance with expectations, taking into consideration that the measured time constant of the fluorescence in the olive oil sample was about 3ns (see Fig. 10).

In addition, we have shown here that it is possible to enhance the fluorescence suppression further by estimating the number of residual fluorescence photons within the time gate used based on the fluorescence tails measured at each of the spectral points. It is important, however, to note that while time gate-based fluorescence suppression improves the signal-to-noise ratio, the latter method acts only as a baseline correction, without affecting the SNR in the sense implied in Eq. (1).

It should also be noted that time-gating does not suppress fluorescence only but also other background-induced phenomena, and especially the dark counts of the detector itself. The dark count rate with a CMOS SPAD, for example, is typically 100-10kHz depending on the details of the detector and technology used. With a time gate of 500ps, an inherent dark count rate of 10kHz and a laser pulsing frequency of 100kHz, for example, the "effective dark count rate" will be reduced to 0.5/second. In the above measurements the effective dark count rate measured with a 300ps time gate and 100kHz pulsing rate was 0.4-0.5 counts/second. With this time gate it would mean that the probability of a dark count detection within the whole Raman spectrum would be around 0.3%.

From practical point of view an important additional advantage of CMOS SPAD techniques is that the detector can be realized as a 2D array. Thus while the measurement time for a single pixel in the above measurements was 40 to 240 seconds, a much wider spectrum could be measured within the same time with a 2D SPAD array. Then, of course, the timing homogeneity and complexity of the chip pose challenges with respect to the realizable time gate widths and number of spectral points as discussed in [12–14], for example. The total measurement time could be further shortened by increasing the average power of the laser used (peak power and/or pulsing rate) and the effective area of the SPAD array (more detectors per spectral point).

The limitations of the proposed technique arise from its modest photon detection efficiency and the fill factor of the CMOS SPAD detector array. Quite promising results have nevertheless been achieved recently when trying to improve the detection efficiency of CMOS SPAD detectors [19]. The fact that the active detector surface is smaller than the whole die area of the detector pixel (including pixel electronics, fill factor) reduces the recorded amount of photons and affects thus onto the measurement time. Micro-lens arrays should be helpful for enlarging the effective active area, however [20].

In the light of the results presented here, we believe that the suggested CMOS SPAD-based time-gating techniques could help us to make better use of the high resolving power of Raman spectrometer techniques in their potential fields of application in the agriculture, food and oil industries and in security control and crime investigations, for example.

Acknowledgments

The authors would like to acknowledge financial support from TEKES (contract nos. 40133/09 and 40115/12) and Academy of Finland (contract nos. 255359, 263705 and 251571).